Pramana – J. Phys. (2020) 94:61
https://doi.org/10.1007/s12043-020-1924-y

MHD mixed convection flow of a nanofluid past a stretching surface of variable thickness and vanishing nanoparticle flux

SUDIPTA GHOSH and SWATI MUKHOPADHYAY*

Department of Mathematics, The University of Burdwan, Burdwan 713 104, India
*Corresponding author. E-mail: swati_bumath@yahoo.co.in

MS received 20 August 2019; revised 13 December 2019; accepted 19 December 2019

Abstract. This article aims to present the flow and heat transfer characteristics of a nanofluid past an elastic sheet having variable thickness in the presence of a magnetic field. Vanishing nanoparticle flux at the boundary has been taken into account for the passive control of nanoparticles. Two-phase model for the nanofluid has been considered. With the help of similarity transformations, the governing nonlinear partial differential equations are converted into nonlinear ordinary differential equations along with the appropriate boundary conditions. The reduced equations are then solved numerically. The effects of buoyancy parameter, magnetic parameter, Brownian motion, thermophoresis parameter etc. on velocity, temperature and nanoparticle volume fraction are presented graphically and analysed in detail. Velocity, temperature and nanoparticle volume fraction are decreasing functions of wall thickness parameter for decelerated flow. Due to increasing values of thermophoresis parameter, the rate of heat transfer at the surface reduces while with the increase in the Brownian motion parameter the mass transfer rate at the surface increases.

Keywords. Nanofluid; magnetic parameter; elastic sheet; variable thickness of the sheet; Brownian motion; thermophoresis effect.

PACS Nos **47.15.Cb; 47.5.P−; 44.20.+b; 47.65.+a**

1. Introduction

Boundary layer flow of the nanofluid over a sheet has gained considerable attention of researchers due to its importance in many industrial applications. The term nanofluid denotes a liquid in which nanoscale particles are suspended in a base fluid with low thermal conductivity such as water, oils and ethylene glycol. Choi [1] first used the term nanofluids to represent a fluid with suspended nanoparticles. Heat transfer enhancement of nanofluids was observed by Xuan and Li [2]. Buongiorno [3] first discussed the convective transport in nanofluids. Kuznetsov and Nield [4] studied the natural convective boundary layer flow of a nanofluid past a vertical plate. Boundary-layer flow of a nanofluid past a stretching sheet was studied by Khan and Pop [5]. Natural convection flow of a nanofluid over a vertical plate with uniform surface heat flux was examined by Khan and Aziz [6]. Rana and Bhargava [7] discussed the flow and heat transfer of a nanofluid over a nonlinearly stretching sheet. In [8–14], other results on nanofluids can be found.

Yirga and Shankar [15] reported the combined effects of magnetic field and porous medium on the nanofluid flow in the presence of viscous dissipation and chemical reaction. Recently, Usman *et al* [16] investigated the effects of unsteadiness and magnetic field on the naofluid flow and heat transfer using differential transform method.

Heat transfer in the flow over a stretching surface having variable thickness has applications in industrial and technological processes. It is quite obvious that the stretching sheet of uneven thickness seems to be more practical than the flat stretching surface (Hayat *et al* [18]). Boundary-layer flow over a stretching sheet with variable thickness was studied by Fang *et al* [17]. Subhashini *et al* [19] investigated the thermal diffusive flow over a stretching sheet with variable thickness. She observed that dual solutions occurred for a certain range of wall thickness parameter. Elbashbeshy *et al* [20] reported the nanofluid flow past a nonlinear stretching sheet of variable thickness. Slip effects on the boundary layer flow due to a stretched surface of variable thickness were reported by Khader and Megahed [21]. Boundary-layer flow due to a stretching

Published online: 01 April 2020

sheet with variable thickness and slip velocity was studied by Khader and Megahed [22]. Impact of Cattaneo–Christov heat flux on the flow over a stretching sheet with variable thickness was analysed by Hayat *et al* [23]. Abdel-Wahed *et al* [24] presented the effects of heat source on the nanofluid flow due to a stretched surface of variable thickness in the presence of a magnetic field. Prasad *et al* [25] analysed the effects of magnetic field and Hall current on a flow past a stretched surface of variable thickness. Vajravelu *et al* [26] examined the characteristics of flow and heat transfer of a rotating fluid over a slender elastic surface of variable thickness in the presence of magnetic field with Hall currents. Prasad *et al* [27] reported the effects of variable fluid properties on the flow past a stretched surface of variable thickness. Hayat *et al* [28] analysed the effects of Cattaneo-Christov heat flux on the flow due to a stretched sheet of variable thickness near a stagnation point. Prasad *et al* [29] discussed about the flow and heat transfer in a nanofluid over a slender elastic sheet with variable thickness. Sheet with variable thickness helps to advance the applications of elastic materials and also helps to diminish the load of structural elements (Hayat *et al* [18]). Yet, sufficient work on sheet with variable thickness are available in open literature.

Effects of buoyancy force on the Newtonian/non-Newtonian fluid flow and heat transfer over a stretching sheet were studied by several researchers. The combined forced and free convection flow is known as mixed convection flow. It has wider applications in industries and technologies. Vajravelu [30] studied convection heat transfer at a stretching sheet in the presence of suction or blowing. Convective heat transfer in an electrically conducting fluid at a stretching surface with uniform free stream was studied by Vajravelu and Hadjinicolaou [31]. Makinde and Aziz [32] examined mixed convection from a vertical plate embedded in a porous medium with a convective boundary condition. Of late, Nabwey *et al* [33] analysed the mixed convection flow of non-Newtonian nanofluid near a stagnation point using group theoretic approach. Waqas *et al* [34] discussed the combined effects of variable fluid properties and mixed convection on non-Newtonian Carreau fluid near a stagnation point. Vajravelu *et al* [35] examined the combined buoyancy effects on the flow, heat and mass transfer of non-Newtonian fluid obeying Ostwald–de Waele model in the presence of chemical reaction.

In those investigations related to surface of variable thickness, effects of buoyancy force were not considered. But for flow passing through vertical surfaces, buoyancy forces cannot be disregarded. As far as the authors know, no attempt has been made yet to report the effects of buoyancy force on nanofluid flow past a vertical surface of variable thickness. Keeping this in mind, an attempt is made in this article to address this. In this model, nanoparticles (> 10 nm) are suspended in the base fluid. As a result, nanoparticles and the fluid lie in different phases: particles are in solid phase whereas the base fluid is in liquid phase. For this reason, the model under consideration is also known as two-phase model. In the present problem, the effects of buoyancy force on the flow and heat transfer of a nanofluid over a power-law stretching sheet of variable thickness in the presence of transverse magnetic field with zero nanoparticle flux at the boundary (for passive control of nanoparticles) have been investigated. Using the appropriate similarity transformations, self-similar solutions of the problem have been obtained and the numerical solutions of the problem are presented. Graphical representations of the results are presented for the leading parameters and analysed in detail.

2. Mathematical formulation of the problem

Consider a steady two-dimensional boundary layer flow of an electrically conducting nanofluid over an impermeable power-law stretching vertical sheet with variable thickness in the presence of magnetic field and buoyancy force. It is assumed that the sheet is not flat, it is of variable thickness and the thickness of the sheet varies with the distance (from the origin) due to increase/decrease in speed of the sheet. It is also assumed that the induced magnetic field, the external electric field and the electric field due to the polarisation of charges are negligible. Moreover, the zero volume fraction flux of the nanoparticles is maintained by the stretching sheet at the boundary. The governing boundary layer equations can be expressed as

$$\frac{\partial u}{\partial x} + \frac{\partial \upsilon}{\partial y} = 0, \tag{1}$$

$$u\frac{\partial u}{\partial x} + \upsilon\frac{\partial u}{\partial y} = \nu\frac{\partial^2 u}{\partial y^2} - \frac{\sigma B^2}{\rho_f}u + g\beta(T - T_\infty), \tag{2}$$

$$u\frac{\partial T}{\partial x} + \upsilon\frac{\partial T}{\partial y} = \kappa\frac{\partial^2 T}{\partial y^2} + \frac{(\rho c)_p}{(\rho c)_f}\left[D_B\frac{\partial C}{\partial y}\frac{\partial T}{\partial y} + \frac{D_T}{T_\infty}\left(\frac{\partial T}{\partial y}\right)^2\right], \tag{3}$$

$$u\frac{\partial C}{\partial x} + \upsilon\frac{\partial C}{\partial y} = D_B\frac{\partial^2 C}{\partial y^2} + \frac{D_T}{T_\infty}\frac{\partial^2 T}{\partial y^2}, \tag{4}$$

where u, υ are the velocity components in x and y directions respectively, ν is the kinematic viscosity, ρ_f is the density of the fluid, σ is the electrical conductivity, $B^2 = B_0^2(1 + x)^{1-m}$ represents the magnetic field

(B_0 which is a constant is the preliminary strength of the magnetic field), g is the acceleration due to gravity, β is the volumetric thermal expansion coefficient, T is the temperature of the fluid, κ denotes the thermal diffusivity, $(\rho c)_p$ is the effective heat capacity of the nanoparticles and $(\rho c)_f$ is the effective heat capacity of the nanofluid, D_{B} and D_{T} are respectively the Brownian diffusion coefficient and thermophoretic diffusion coefficient, C is the nanoparticle volume fraction and T_∞ is the constant temperature of the fluid in inviscid free stream.

The boundary conditions are given by

$$u = U_w = U_0(x+b)^m, \quad \upsilon = 0, \quad T = T_w,$$

$$D_{\mathrm{B}}\frac{\partial C}{\partial y} + \frac{D_{\mathrm{T}}}{T_\infty}\frac{\partial T}{\partial y} = 0 \quad \text{at} \quad y = A(x+b)^{\frac{1-m}{2}} \tag{5}$$

$$u \to 0,\ T \to T_\infty,\ C \to C_\infty \quad \text{as} \quad y \to \infty, \tag{6}$$

where U_0 is a constant which stands for reference velocity, b is a dimensionless constant related to the stretching sheet, m is the shape parameter which controls the shape of the surface, U_w is the velocity component stretching along the x directions, T_w is the uniform temperature of the surface and C_∞ is a constant which stands for the nanoparticle volume fraction in inviscid free stream. As the sheet is not flat, it is considered that its thickness varies as $y = A(x+b)^{(1-m)/2}$ where A is a constant. To keep away from a quantifiable pressure gradient along the sheet, the value of A is to be taken very small so that the sheet becomes sufficiently thin.

In the present problem we shall consider $m \neq 1$ as the problem reduces to a problem related to the flat sheet for $m = 1$. The thickness of the sheet increases for $m < 1$ and is responsible for outer convex-type shape whereas thickness of the sheet decreases when $m > 1$ which is responsible for the inner concave-type shape (Hayat *et al* [36]).

2.1 *Self-similar solutions*

Let us now introduce the stream function ψ and the similarity transformations as follows:

$$u = \frac{\partial \psi}{\partial y}, \quad \upsilon = -\frac{\partial \psi}{\partial x}, \quad \psi = F(\zeta)\sqrt{\frac{2}{m+1}\upsilon U_0(x+b)^{m+1}},$$

$$\zeta = y\sqrt{\frac{(m+1)}{2\upsilon}U_0(x+b)^{m-1}}, \tag{7}$$

where

$$u = \frac{\partial \psi}{\partial y}, \quad \upsilon = -\frac{\partial \psi}{\partial x}$$

and ζ is the similarity variable.

Equation (1) is automatically satisfied by this.

$$u = U_0(x+b)^m F'(\zeta),$$

$$\upsilon = -\sqrt{\frac{\upsilon(m+1)}{2}U_0(x+b)^{m-1}} \times\left[F(\zeta) + \zeta F'(\zeta)\left(\frac{m-1}{m+1}\right)\right],$$

$$\vartheta(\zeta) = \frac{T - T_\infty}{T_w - T_\infty}, \quad \varphi(\zeta) = \frac{C - C_\infty}{C_w - C_\infty}. \tag{8}$$

Using relations (7) and (8) in eqs (2)–(4), we get the following equations:

$$F''' + FF'' - \frac{2m}{m+1}F'^2 - MF' + \lambda\vartheta = 0, \tag{9}$$

$$\vartheta'' + \mathrm{Pr}(F\vartheta' + N_{\mathrm{b}}\vartheta'\varphi' + N_{\mathrm{t}}\vartheta'^2) = 0, \tag{10}$$

$$\varphi'' + \mathrm{Le}(F\varphi') + \frac{N_{\mathrm{t}}}{N_{\mathrm{b}}}\vartheta'' = 0. \tag{11}$$

The dimensionless parameter

$$\lambda = \frac{2g\beta d}{U_0 l^{2m-1}(m+1)}$$

represents the buoyancy or free convection parameter. Here, $\lambda > 0$ assists the flow, whereas $\lambda < 0$ opposes the flow. $\lambda = 0$ represents the case when there is no buoyancy force. Moreover, $\lambda > 1$ represents the case of free convection or natural convection whereas $\lambda < 1$ presents the case of forced convection flow. Here

$$\mathrm{Pr} = \frac{\upsilon}{\kappa}$$

is the Prandtl number

$$\mathrm{Le} = \frac{\upsilon}{D_{\mathrm{B}}}$$

is the Lewis number,

$$M = \frac{2\sigma B_0^2}{\rho_f U_0(m+1)}$$

is the magnetic parameter,

$$N_{\mathrm{b}} = \frac{(\rho c)_p(C_w - C_\infty)D_{\mathrm{B}}}{(\rho c)_f \upsilon}$$

is the Brownian motion parameter and

$$N_{\mathrm{t}} = \frac{(\rho_c)_p D_{\mathrm{T}}(T_w - T_\infty)}{(\rho_c)_f \upsilon T_\infty}$$

is the thermophoresis parameter.

Table 1. Values of $-f''(0)$ for various values of M when $m = 1$ and $\lambda = 0$.

	$M = 0$	$M = 0.5$	$M = 1.0$	$M = 1.5$	$M = 2.0$
Exact results	1.000	1.2247	1.414235	1.5811388	1.732050
Results of Andersson *et al* [38]	1.00000	1.2249	1.4140	1.58100	1.73200
Results of Hsiao [39]	1.00000	1.2249			
Results of Prasad *et al* [27]	1.000174	1.224793	1.414499	1.581139	1.732203
Present results	1.00000	1.224782	1.414487	1.581026	1.732205

The transformed boundary conditions are

$$F(\alpha) = \alpha\frac{1-m}{1+m}, \quad F'(\alpha) = 1, \quad \vartheta(\alpha) = 1,$$

$$N_b\varphi'(\alpha) + N_t\vartheta'(\alpha) = 0, \tag{12}$$

$$F'(\infty) = 0, \quad \vartheta(\infty) = 0, \quad \varphi(\infty) = 0, \tag{13}$$

where α denotes the wall thickness parameter.

In order to facilitate the computation, let us introduce the function

$$f(\eta) = f(\zeta - \alpha) = F(\zeta),$$
$$\theta(\eta) = \theta(\zeta - \alpha) = \vartheta(\zeta), \quad \phi(\eta) = \phi(\zeta - \alpha) = \varphi(\zeta).$$

Here $\zeta = \alpha$ indicates the plate surface.

Now, eqs (9)–(11) become

$$f''' + ff'' - \frac{2m}{m+1}f'^2 - Mf' + \lambda\theta = 0, \tag{14}$$

$$\theta'' + \Pr(f\theta' + N_b\theta'\phi' + N_t\theta'^2) = 0, \tag{15}$$

$$\phi'' + \mathrm{Le}(f\phi') + \frac{N_t}{N_b}\theta'' = 0. \tag{16}$$

The boundary conditions become:

$$f(0) = \alpha\frac{1-m}{1+m}, \quad f'(0) = 1, \quad \theta(0) = 1,$$

$$N_b\phi'(0) + N_t\theta'(0) = 0, \tag{17}$$

$$f'(\infty) = 0, \quad \theta(\infty) = 0, \quad \phi(\infty) = 0. \tag{18}$$

The first boundary condition

$$f(0) = \frac{1-m}{1+m}\alpha$$

given by (17) indicates that three cases may arise: $m < 1$, $m = 0$ and $m > 1$.

For $-1 < m < 1$, $f(0) > 0$ which represents the case of suction, for $m = 0$, $f(0) = 0$ which represents the case of impermeable surface and for $m > 1$, $f(0) < 0$ which represents the case of injection at the boundary.

For this problem the quantities of interest are the local skin friction coefficient, the local Nusselt number and the local Sherwood number which are defined as

$$C_{f_x} = \frac{2\nu(\partial u/\partial y)_{y=A(x+b)^{\frac{1-m}{2}}}}{U_w^2},$$

$$\mathrm{Nu}_x = \frac{(x+b)(\partial T/\partial y)_{y=A(x+b)^{\frac{1-m}{2}}}}{(T_w - T_\infty)},$$

$$\mathrm{Sh}_x = \frac{(x+b)(\partial C/\partial y)_{y=A(x+b)^{\frac{1-m}{2}}}}{(C_w - C_\infty)}$$

$$C_{f_x} = 2\sqrt{(m+1)/2}\mathrm{Re}_x^{-1/2}f''(0),$$

$$\mathrm{Nu}_x = -\sqrt{(m+1)/2}\mathrm{Re}_x^{1/2}\theta'(0),$$

$$\mathrm{Sh}_x = -\sqrt{(m+1)/2}\mathrm{Re}_x^{1/2}\phi'(0), \tag{19}$$

where

$$\mathrm{Re}_x = \frac{U_w(x+b)}{\nu}$$

is the local Reynolds number.

2.2 *Exact solutions for some particular cases*

Exact solutions are always important and useful which will help to compare and validate our numerical results. We are interested to find exact solutions for some particular cases in the absence of buoyancy force. So we shall consider $\lambda = 0$ in all cases for finding exact solutions.

Case I: *Flow past a flat plate in the absence of magnetic field*

Here, $m = 1, b = 0$ and $M = 0$. Thus, eq. (14) becomes

$$f''' + ff'' - f'^2 = 0.$$

The corresponding boundary conditions take the following form:

$$f(0) = 0, \quad f'(0) = 1 \text{ and } f'(\infty) = 0.$$

The corresponding solution is $f(\eta) = 1 - \mathrm{e}^{-\eta}$ which agrees well with the result of Andersson [37].

Table 2. Comparison of results for $-f''(0)$ when $M = 0$ and $\lambda = 0$.

α	m	Fang *et al* [17] by shooting method	Khader and Megahed [21]	Present work
0.5	9	1.0589	1.0588	1.05892
	7	1.0550	1.0551	1.05507
	5	1.0486	1.0486	1.04863
	3	1.0359	1.0358	1.03592
	2	1.0234	1.0234	1.02341
	0.5	0.9799	0.9798	0.97995
	0	0.9576	0.9577	0.95763
	$-1/3$	1.0000	1.0000	1.0000
	$-1/2$	1.1667	1.1666	1.16675
0.25	9	1.1404	1.1404	1.14047
	7	1.1323	1.1323	1.13235
	5	1.1186	1.1186	1.11864
	3	1.0905	1.0904	1.09054
	0.5	0.9338	0.9337	0.93382
	0	0.7843	0.7843	0.78435
	$-1/3$	0.5000	0.5000	0.5000
	$-1/2$	0.0833	0.08322	0.08333

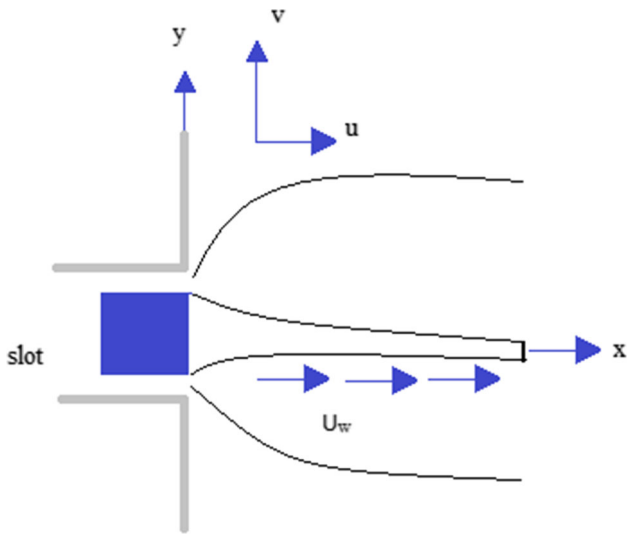

Figure 1. Sketch of the physical problem.

Case II: *Flow past a flat plate in the presence of magnetic field*

Here, $m = 1$ and $b = 0$. Thus, eq. (14) now becomes

$$f''' + ff'' - f'^2 - Mf' = 0.$$

The corresponding boundary conditions take the following form:

$$f(0) = 0, \quad f'(0) = 1 \quad \text{and} \quad f'(\infty) = 0.$$

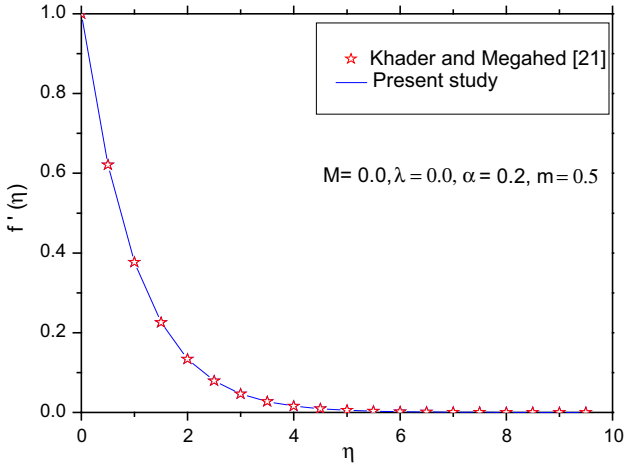

Figure 2. Comparison of the velocity profiles.

The solution for the velocity field is given by

$$f(\eta) = \frac{1}{\sqrt{1+M}}\left(1 - e^{-\sqrt{1+M}\,\eta}\right)$$

which agrees well with the findings of Andersson *et al* [38] for Newtonian fluid and Hsiao [39] in the absence of viscoelastic parameter.

2.3 *Numerical solutions of the problem*

The governing equations (14)–(16) subject to the boundary conditions (17) and (18) are solved numerically using Runge–Kutta method with the help of shooting technique. To find out the appropriate finite value of η_∞ is the main problem for this method. Here this value ($\eta_\infty = 5$) is chosen very carefully so that the far-field boundary conditions given by (18) are satisfied asymptotically.

3. Results and discussions

3.1 *Verification of numerical results*

To authenticate the numerical results acquired in this investigation, our results are compared with the existing results of Andersson *et al* [38] (for $n = 1$), Hsiao [39] (in the absence of viscoelastic parameter) (for $E = 0$), Prasad *et al* [27] (for $m = 1, \theta_r \to \infty, \varepsilon = 0$) and also with the exact results available for the particular case of flat plate. The results obtained in the present study agree completely with these results (see table 1). Moreover, an assessment is made with the available results of Fang *et al* [17], Khader and Megahed [21] for some

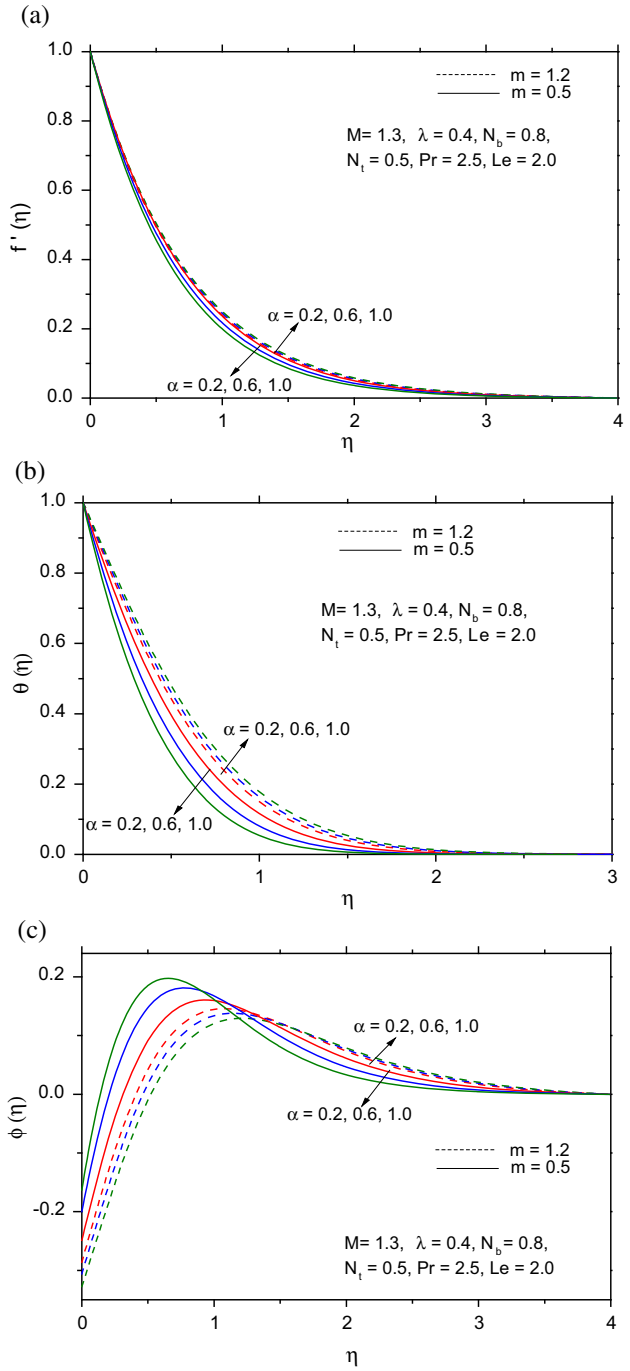

Figure 3. Effect of α on (**a**) velocity $f'(\eta)$, (**b**) temperature $\theta(\eta)$ and (**c**) nanoparticle volume fraction $\phi(\eta)$.

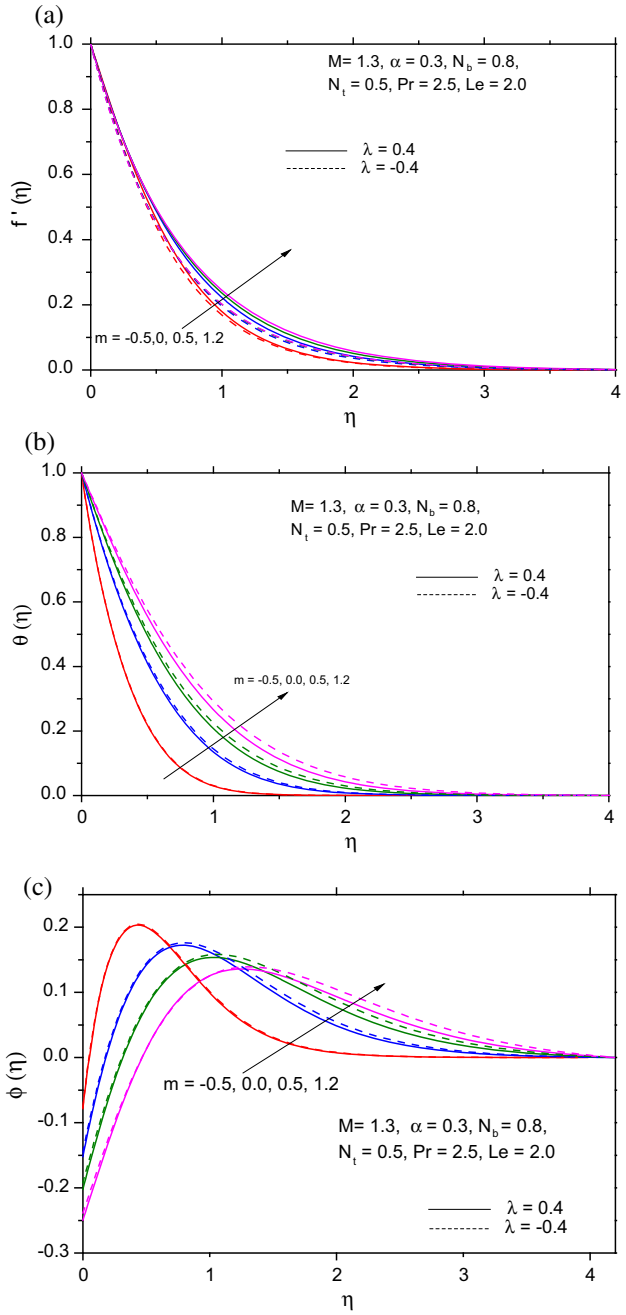

Figure 4. Effect of m on (**a**) $f'(\eta)$, (**b**) $\theta(\eta)$ and (**c**) $\phi(\eta)$.

particular values of the governing parameters and presented in table 2 which shows a good agreement with the existing results (figures 1, 2).

3.2 *Analysis of the results*

The effects of surface thickness parameter (α) for buoyancy-aided flow for two cases of shape parameter m ($m = 0.5 < 1$ and $m = 1.2 > 1$) are observed on velocity, temperature and nanoparticle volume fraction and are depicted respectively in figures 3a–3c. Figure 3a shows that the velocity decreases for buoyancy-aided flow with the rise in α for $m = 0.5$. Basically, as the thickness of the sheet increases, elongation of the surface decreases. As a result, velocity of the fluid reduces for $m = 0.5$ (figure 3a). But opposite trend of velocity is noted for $m = 1.2$. As the thickness of the sheet decreases, elongation of the surface increases which is responsible for the increase of velocity with the rise in α (figure 3a). The velocity decreases initially for the

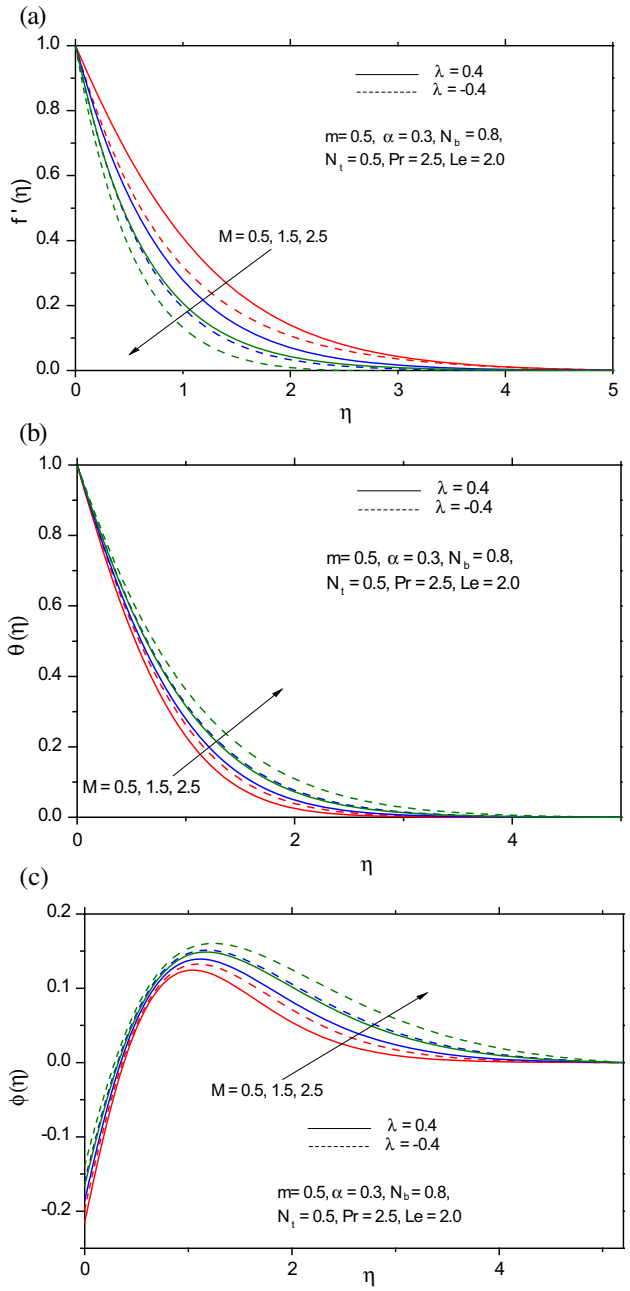

Figure 5. Effect of M on (**a**) $f'(\eta)$, (**b**) $\theta(\eta)$ and (**c**) $\phi(\eta)$.

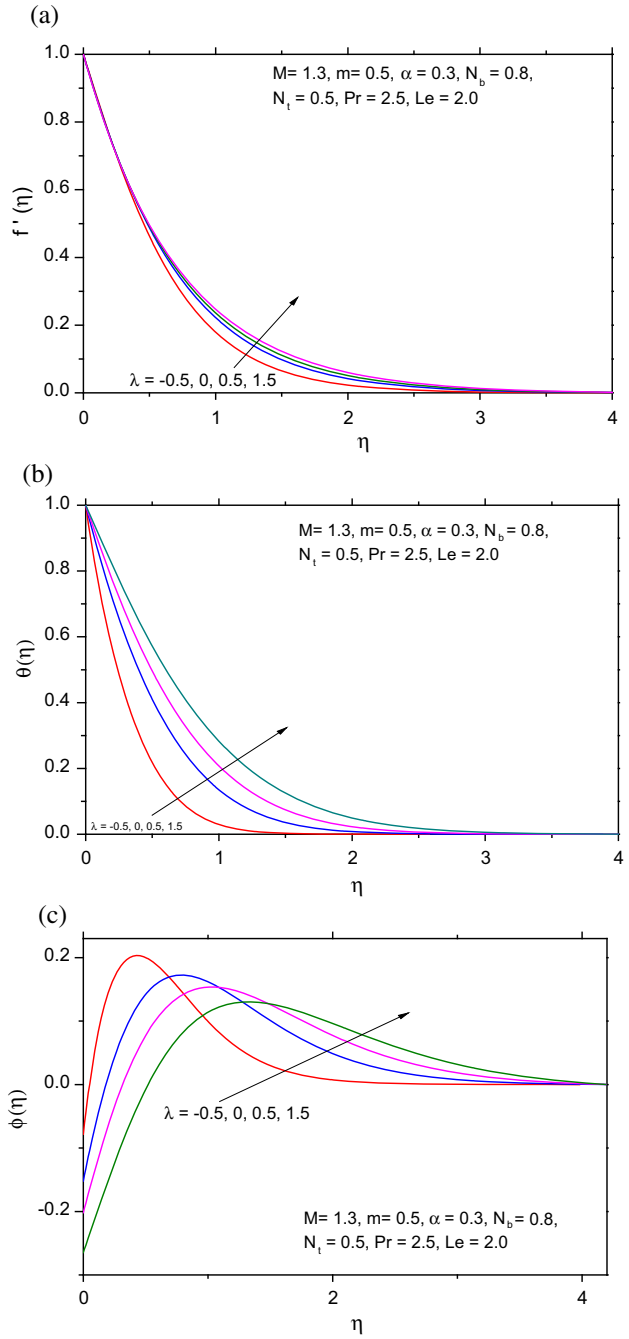

Figure 6. Effect of λ on (**a**) $f'(\eta)$, (**b**) $\theta(\eta)$ and (**c**) $\phi(\eta)$.

buoyancy-opposed forces but away from the sheet, fluid velocity increases. Temperature decreases with the rising values of α when $m = 0.5$ (figure 3b). The result is quite obvious as in this case the thickness of the sheet enhances. But reverse trend of temperature is noted for $m = 1.2$ (figure 3b). The nanoparticle volume fraction increases initially with α but it decreases finally with α for $m = 0.5$ but opposite trend is noted for $m = 1.2$ for buoyancy-aided flow (figure 3c). Same type of behaviour of nanoparticle volume fraction is noted for buoyancy-opposed flow.

The shape parameter (m) also controls the fluid motion. The motion becomes decelerated for $m < 1$ and accelerated for $m > 1$. For $m = 0$ the motion is linear with constant velocity (Hayat *et al* [28]). The effects of m on velocity, temperature and nanoparticle volume fraction are presented in figures 4a–4c. For the buoyancy-aided flow, the fluid velocity is found to decrease initially but increases away from the sheet with m (figure 4a). Fluid velocity is higher for buoyancy-aided flow compared to that for buoyancy-opposed flow

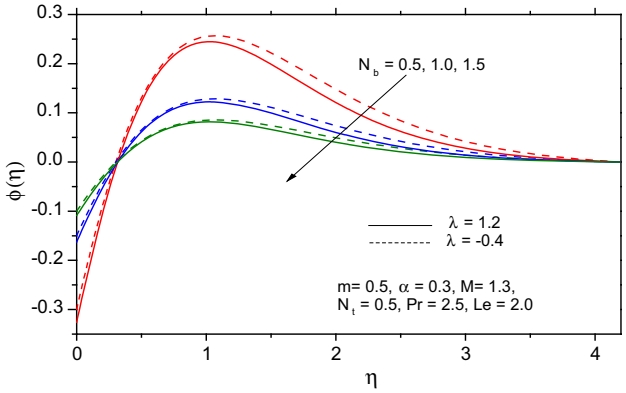

Figure 7. Effect of N_b on $\phi(\eta)$.

(figure 4a). Temperature increases due to the increase in m for both buoyancy-aided and buoyancy-opposed flows (figure 4b). Higher temperature is noted for buoyancy-opposed flow. Near the sheet, nanoparticle volume fraction decreases with the increase in m but finally it increases (figure 4c).

The effects of magnetic parameter (M) on velocity, temperature and nanoparticle volume fraction are depicted respectively in figures 5a–5c. Velocity decreases for both buoyancy-aided and buoyancy-opposed flows (figure 5a). A dealing force named as Lorentz force grows due to the interaction of transverse magnetic field with the conducting nanofluid. Such force helps to slow down the fluid motion and to shrink the momentum boundary layer. It is observed that fluid velocity is highest for hydrodynamic case (i.e. for $M = 0$) compared to hydromagnetic case ($M > 0$) which is obvious. Both temperature (figure 5b) and nanoparticle volume fraction (figure 5c) increase for the increase in M. Lorentz force makes the thermal boundary layer (figure 5b) and nanoparticle volume fraction layer (figure 5c) thicker in the region of flow.

Physically, $\lambda > 0$ corresponds to the warming of the fluid or cooling of the surface, $\lambda < 0$ corresponds to the cooling of the fluid or warming of the surface and $\lambda = 0$ corresponds to the case when there is no free convection currents. As a result, due to increase in the buoyancy parameter (λ), the fluid velocity increases (figure 6a) because increase in λ leads to an increase in the temperature difference ($T_w - T_\infty$) leading to the enhancement of velocity in the x direction. Basically, for $\lambda > 0$ an additional buoyancy-induced flow occurs. As a result, fluid velocity increases and an enhancement in the momentum boundary layer thickness is noted (figure 6a). Both temperature (figure 6b) and nanoparticle volume fraction (figure 6c) increase when λ increases.

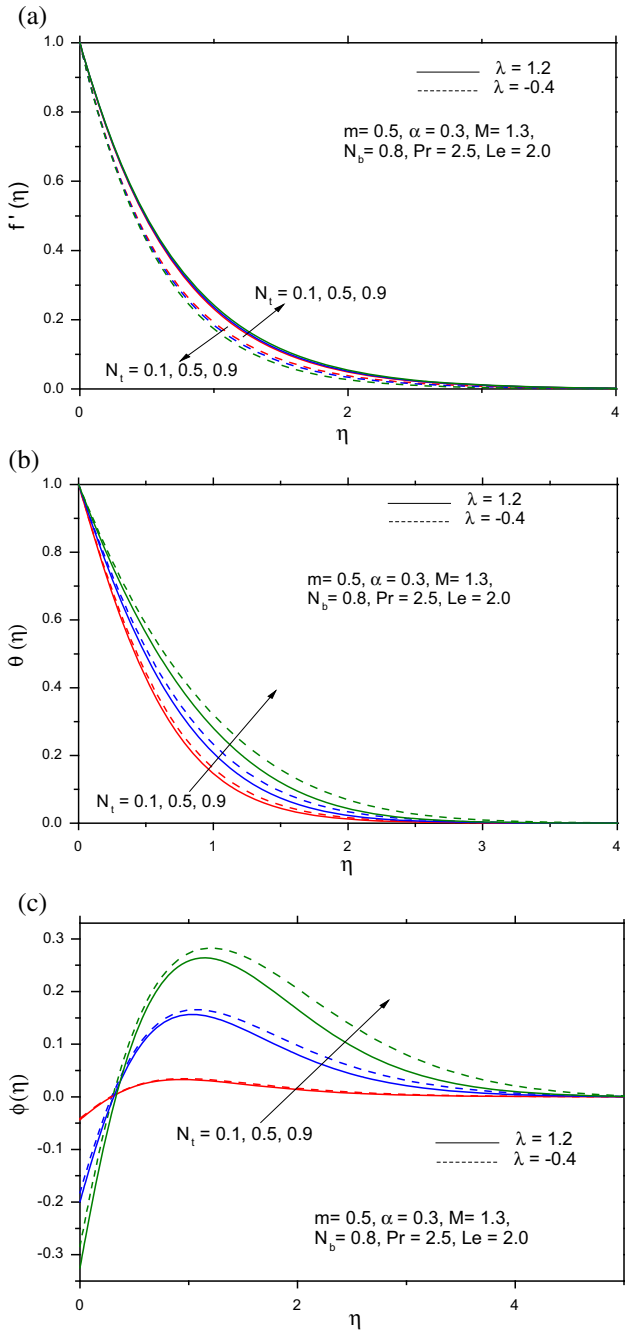

Figure 8. Effect of N_t on (**a**) $f'(\eta)$, (**b**) $\theta(\eta)$ and (**c**) $\phi(\eta)$.

As the Brownian motion parameter (N_b) increases, the random motion of the nanoparticles due to the collision between the particles increases. As a result, temperature and thermal boundary layer thickness increase. As the result is not so significant, it is not provided here. Nanoparticle volume fraction finally decreases with the rise in N_b (figure 7) which is also observed by Prasad *et al* [29]. Basically, higher values of N_b suppress the diffusion of nanoparticles away from the surface [29]. So, within the boundary layer the nanoparticle volume fraction decreases.

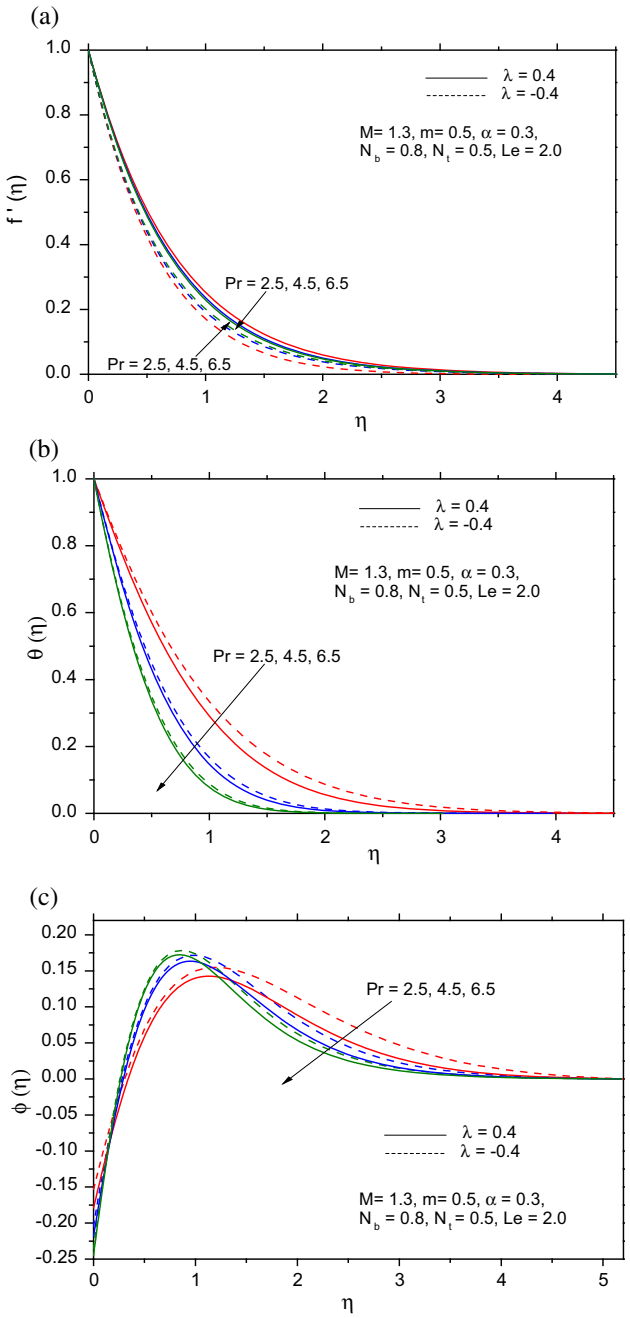

Figure 9. Effect of Pr on (**a**) $f'(\eta)$, (**b**) $\theta(\eta)$ and (**c**) $\phi(\eta)$.

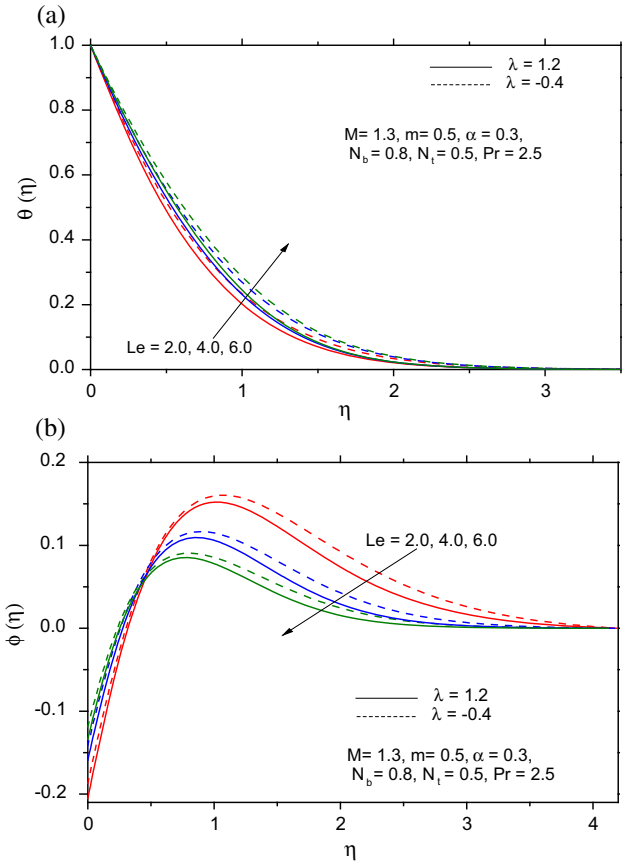

Figure 10. Effect of Le on (**a**) $\theta(\eta)$ and (**b**) $\phi(\eta)$.

It is observed from figure 8a that the velocity increases slightly due to an increase in thermophoresis parameter (N_t) in the case of buoyancy-aided flow but decreases for buoyancy-opposed flow. From figures 8b and 8c it is found that that the boundary-layer thicknesses for temperature and nanoparticle volume fraction both increase due to the increase in N_t. With the rise in N_t, conductivity of the fluid increases rapidly. As a result, temperature of the fluid increases (figure 8b). As N_t increases, the temperature difference between the sheet and the fluid also increases and hence the thermal boundary-layer thickness increases (figure 8b). A noteworthy reduction in the nanoparticle volume fraction near the wall (surface), i.e. for the hot surface is observed (figure 8c). As the warm surface slows down, the nanoparticles structure a comparatively particle-free layer near the hot surface. As a result, the nanoparticle volume fraction decreases near the surface where the surface is hot. As N_t increases, thermophoresis force increases which has a trend to shift particles from warm to cold areas. Due to the increase of nanoparticles, the concentration of the fluid enhances finally (figure 8c). As a result, thickness of the nanoparticle concentration boundary layer increases.

From figure 9a, it is clear that velocity decreases in the buoyancy-aided flow but increases for buoyancy-opposed flow (figure 9a) but temperature (figure 9b) and nanoparticle volume fraction (figure 9c) decrease with the increasing Prandtl number (Pr). With the rise in Pr, thermal diffusivity decreases which helps to reduce the energy transfer in the nanofluid.

The effect of Lewis number (Le) on the dimensionless temperature and nanoparticle volume fraction are depicted in figures 10a and 10b. It is observed that

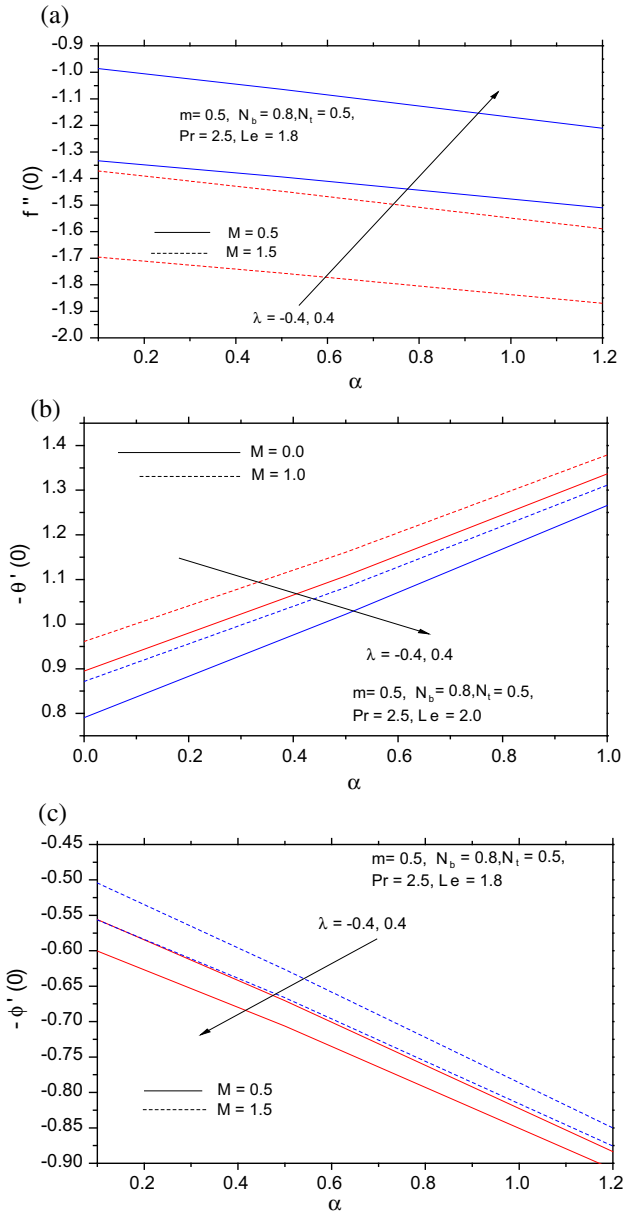

Figure 11. Effects of α, λ and M on (**a**) local skin friction coefficient, (**b**) local Nusselt number and (**c**) local Sherwood number.

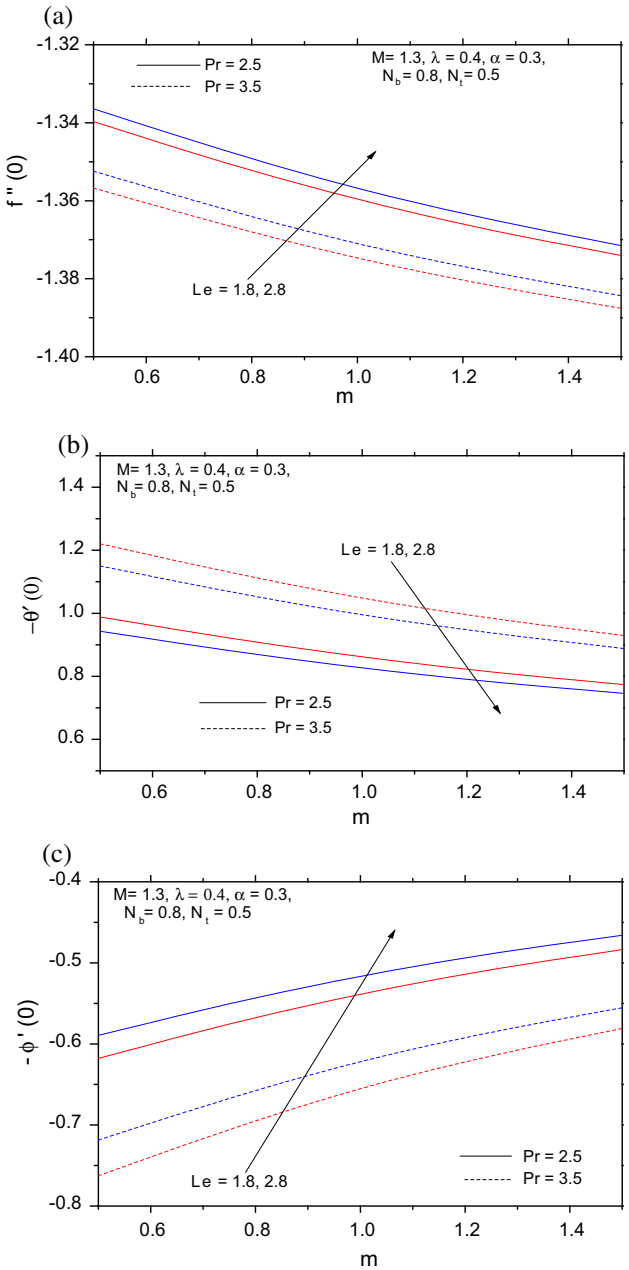

Figure 12. Effects of velocity power index m, Le and Pr on (**a**) local skin friction coefficient, (**b**) local Nusselt number and (**c**) local Sherwood number.

temperature increases (figure 10a) but the nanoparticle volume fraction finally decreases (figure 10b) for both buoyancy-aided and buoyancy-opposed flows with increasing Le. Concentration boundary layer thickness decreases for increasing Le (figure 10b). This is due to the decrease in mass diffusivity or the Brownian motion of the nanoparticle. Actually, Le is the relative amount of the thermal diffusivity to the mass diffusivity.

The values of $f''(0)$, $-\theta'(0)$, $-\varphi'(0)$ vs. α for two different values of λ and M are plotted in figures 11a–11c. Wall shear stress $f''(0)$ decreases with increasing values of α and M but increases with the increasing values of λ (figure 11a). Local Nusselt number $[-\theta'(0)]$ increases with increasing values of λ and also with α but decreases with M (figure 11b) and local Sherwood number is found to decrease with α and λ but increases with M (figure 11c).

Velocity gradient at the wall ($f''(0)$) decreases with increasing m and Pr but increases with Le (figure 12a). Local Nusselt number decreases with Le and also with

Table 3. Values of $f''(0)$, $\theta'(0)$ and $\phi'(0)$ for various values of governing parameters with Pr = 1.23 and Le = 1.8.

				$m = 0.5, \alpha = 0.35$			$m = 1.5, \alpha = 0.70$		
λ	M	N_b	N_t	$f''(0)$	$\theta'(0)$	$\phi'(0)$	$f''(0)$	$\theta'(0)$	$\phi'(0)$
−0.2	0.5	0.3	0.2	−1.30748	−0.669001	0.446001	−1.32336	−0.441962	0.294642
			0.4	−1.31142	−0.634899	0.846533	−1.32634	−0.420582	0.560776
			0.6	−1.31515	−0.601799	1.2036	−1.32964	−0.398499	0.796997
			0.8	−1.31905	−0.569735	1.51929	−1.33337	−0.375389	1.00104
			1.0	−1.32312	−0.538728	1.79576	−1.33779	−0.350504	1.16835
0	1.0	0.5	0.2	−1.39616	−0.661848	0.264739	−1.392	−0.447605	0.179042
			0.6		−0.598478	0.718174		−0.413969	0.496762
			1.0		−0.540941	1.08188		−0.381384	0.762768
			1.4		−0.4865	1.36822		−0.354494	0.992582
			1.8		−0.441935	1.59097		−0.325661	1.17238
0.5	1.5	0.7	0.2	−1.34481	−0.689162	0.196903	−1.33453	−0.501648	0.143328
			0.4	−1.34046	−0.659254	0.376716	−1.33224	−0.487232	0.278418
			0.6	−1.33643	−0.631514	0.541298	−1.33047	−0.475164	0.407284
			0.8	−1.33185	−0.602912	0.689043	−1.32767	−0.458853	0.524403
			1.0	−1.32733	−0.575595	0.822279	−1.32489	−0.442853	0.632646
1.2	2.0	1.1	0.2	−1.23389	−0.719773	0.130868	−1.22179	−0.538361	0.0978838
			0.4	−1.22575	−0.690797	0.251199	−1.219	−0.527891	0.19196
			0.6	−1.21769	−0.662871	0.361566	−1.21487	−0.514382	0.280572
			0.8	−1.20971	−0.63601	0.462553	−1.21074	−0.500977	0.364347
			1.0	−1.20186	−0.610224	0.554749	−1.20662	−0.487702	0.443366

m but increases with higher values of Pr (figure 12b). Brownian diffusion effect increases with the decrease in Le. As a result, heat transfer is higher for lower values of Le. Local Sherwood number increases with m as well as with the rising values of Le but it increases with higher values of Pr (figure 12c).

Table 3 shows that $f''(0)$ decreases with the rise in N_t for buoyancy-opposed flow ($\lambda < 0$) but increases for buoyancy-aided flow ($\lambda > 0$). But the wall temperature gradient $\theta'(0)$ and the nanoparticle volume flux at the wall $\phi'(0)$ both increase with the rising values of N_t for $\lambda < 0$ and $\lambda > 0$, i.e. heat transfer decreases with increase in N_t.

4. Conclusions

Effects of buoyancy force on the magnetohydrodynamic flow of the nanofluid due to a stretched surface of variable thickness have been reported. The main observations are listed below.

(i) Velocity, temperature and nanoparticle volume fraction all are decreasing functions of α for $m < 1$, i.e. for decelerated flow. Opposite is observed for accelerated flow, i.e. for $m > 1$.
(ii) Fluid velocity, temperature and nanoparticle volume fraction all increase with λ for decelerated flow ($m < 1$).
(iii) Velocity increases with the rise in thermophoresis for accelerated motion but decreases for decelerated flow. Temperature and nanoparticle volume fraction are increasing functions of N_t.
(iv) Magnitude of the skin friction coefficient is enhanced for higher values of M.

Acknowledgement

The authors are thankful to the editor and reviewers for their constructive suggestions.

References

[1] S U S Choi, ASME, FED 231/MD, USA **66**, 99 (1995)
[2] Y Xuan and Q Li, *Int. J. Heat Fluid Flow* **21**, 58 (2000)
[3] J Buongiorno, *ASME J. Heat Transfer* **128**, 240 (2006)
[4] A V Kuznetsov and D A Nield, *Int. J. Therm. Sci.* **49**(**2**), 243 (2010)
[5] W A Khan and I Pop, *Int. J. Heat Mass Transfer* **53**, 2477 (2010)
[6] W A Khan and A Aziz, *Int. J. Therm. Sci.* **50**, 1207 (2011)
[7] P Rana and R Bhargava, *Commun. Nonlinear Sci. Numer. Simul.* **17**, 212 (2012)
[8] M Sheikholeslami, B Rezaeianjouybari, M Darzi, A Shafee, Z Li and T K Nguyen, *Int. J. Heat Mass Transfer* **141**, 974 (2019)
[9] M Sheikholeslami, M Jafaryar, A Shafee, Z Li and R ul Haq, *Int. J. Heat Mass Transfer* **136**, 1233 (2019)

[10] M Sheikholeslami, *Comput. Meth. Appl. Mech. Eng.* **344**, 319 (2019)
[11] M Sheikholeslami and O Mahian, *J. Clean. Prod.* **215**, 963 (2019)
[12] M Sheikholeslami, M Jafaryar, M Hedayat, A Shafee, Z Li, T K Nguyen and M Bakouri, *Int. J. Heat Mass Transfer* **137**, 1290 (2019)
[13] M Sheikholeslami, A Arabkoohsar, I Khan, A Shafee and Z Li, *J. Clean. Prod.* **221**, 885 (2019)
[14] S Ghosh and S Mukhopadhyay, *Pramana – J. Phys*. **92**: 93 (2019)
[15] Y Yirga and B Shankar, *Int. J. Comput. Meth. Eng. Sci. Mech.* **16**, 275 (2015)
[16] M Usman, M Hamid, U Khan, S T M Din, M A Iqbal and W Wang, *Alex. Eng. J.* (2017) https://doi.org/10.1016/j.aej.2017.03.052
[17] T Fang, Ji Zhang and Y Zhong, *Appl. Math. Comput.* **218**, 7241 (2012)
[18] T Hayat, I Ullah, A Alsaedi and M Farooq, *Results Phys.* **7**, 189 (2017)
[19] S V Subhashini, R Sumathi and I Pop, *Int. Commun. Heat Mass Transfer* **48**, 61 (2013)
[20] E M A Elbashbeshy, T G Emam and M S Abdel-Wahed, *Can. J. Phys.* **91**, 699 (2013)
[21] M M Khader and A M Megahed, *Eur. Phys. J. Plus* **128**, 100 (2013)
[22] M M Khader and A M Megahed, *J. Appl. Mech. Tech. Phys.* **56(2)**, 241 (2015)
[23] T Hayat, M Farooq, A Alsaedi and F Al-Solamy, *AIP Adv.* **5**, 087159 (2015)
[24] M S Abdel-Wahed, E M A Elbashbeshy and T G Emam, *Appl. Math. Comput*. **254**, 49 (2015)
[25] K V Prasad, K Vajravelu and H Vaidya, *Int. J. Comput. Meth. Eng. Sci. Mech.* **17**(**4**), 288 (2016)
[26] K Vajravelu, K V Prasad, Chiu-On Ng and H Vaidya, *Int. J. Appl. Comput. Math*. (2016), https://doi.org/10.1007/s40819-016-0291-3
[27] K V Prasad, H Vaidya and K Vajravelu, *J. Mech.* (2016), https://doi.org/10.1017/jmech.2016.101
[28] T Hayat, M Zubair, M Ayub, M Waqas and A Alsaedi, *Eur. Phys. J. Plus* **131**, 355 (2016)
[29] K V Prasad, K Vajravelu, H Vaidya and R A Van Gorder, *Results Phys.* **7**, 1462 (2017)
[30] K Vajravelu, *J. Math. Anal. Appl.* **188**, 1002 (1994)
[31] K Vajravelu and A Hadjinicolaou, *Int. J. Eng. Sci.* **35**, 1237 (1997)
[32] O D Makinde and A Aziz, *Int. J. Therm. Sci.* **49**, 1813 (2010)
[33] H A Nabwey, M Boumazgour and A M Rashad, *Indian J. Phys*. (2017), https://doi.org/10.1007/s12648-017-0978-2
[34] M Waqas, A Alsaedi, S A Shehzad, T Hayat and S Asghar, *J. Braz. Soc. Mech. Sci. Eng*. (2017), https://doi.org/10.1007/s40430-017-0743-7
[35] K Vajravelu, K V Prasad, P S Datti and B T Raju, *J. King Saud University – Eng. Sci.* **29**, 57 (2017)
[36] T Hayat, K Muhammad, M Farooq and A Alsaedi, *AIP Adv.* **6**, 015214 (2016)
[37] H I Andersson, *Acta Mech.* **158**, 121 (2002)
[38] H I Andersson, K H Bech and B S Dandapat, *Int. J. Non-Linear Mech*. **27**, 929 (1992)
[39] K L Hsiao, *Commun. Nonlinear Sci. Numer. Simul.* **15**, 1803 (2010)